Journal of Structural Geology 32 (2010) 1629–1642

Contents lists available at ScienceDirect

Journal of Structural Geology

journal homepage: www.elsevier.com/locate/jsg

Analysis of the growth of strike-slip faults using effective medium theory

Atilla Aydin [a,*], James G. Berryman [b]

[a] Rock Fracture Project, Department of Geological and Environmental Sciences, Stanford University, Stanford, CA, USA
[b] Lawrence Berkeley National Laboratory, Earth Science Division, One Cyclotron Road, MS/90R1116, Berkeley, CA, USA

ARTICLE INFO

Article history:
Received 14 March 2009
Received in revised form
9 November 2009
Accepted 16 November 2009
Available online 27 November 2009

Keywords:
Fault growth
Fault scaling
Fault linkage and coalescence
Fault damage zone
Cataclastic deformation
Effective moduli
Effective medium model

ABSTRACT

Increases in the dimensions of strike-slip faults including fault length, thickness of fault rock and the surrounding damage zone collectively provide quantitative definition of fault growth and are commonly measured in terms of the maximum fault slip. The field observations indicate that a common mechanism for fault growth in the brittle upper crust is fault lengthening by linkage and coalescence of neighboring fault segments or strands, and fault rock-zone widening into highly fractured inner damage zone via cataclastic deformation. The most important underlying mechanical reason in both cases is prior weakening of the rocks surrounding a fault's core and between neighboring fault segments by faulting-related fractures. In this paper, using field observations together with effective medium models, we analyze the reduction in the effective elastic properties of rock in terms of density of the fault-related brittle fractures and fracture intersection angles controlled primarily by the splay angles. Fracture densities or equivalent fracture spacing values corresponding to the vanishing Young's, shear, and quasi-pure shear moduli were obtained by extrapolation from the calculated range of these parameters. The fracture densities or the equivalent spacing values obtained using this method compare well with the field data measured along scan lines across the faults in the study area. These findings should be helpful for a better understanding of the fracture density/spacing distribution around faults and the transition from discrete fracturing to cataclastic deformation associated with fault growth and the related instabilities.

1. Introduction

Strike-slip faults, similar to other types of faults, typically have complex architectures with numerous segments or strands of various trace lengths separated by steps or relays of various sizes (Fig. 1a). This discontinuous characteristic of strike-slip faults has been reported for simple incipient faults (Segall and Pollard, 1980, 1983; Gamond, 1983; Sibson, 1986; Willemse et al., 1997; Peacock and Sanderson, 1995) as well as for mature crustal-scale faults (Aydin and Nur, 1982; Barka and Kadinsky-Cade, 1988; Wesnousky, 1988; Stirling et al., 1996; Kim et al., 2004) and is thought to be pertinent to a number of properties of strike-slip fault systems including their permeability structure (Sibson, 1985; Martel and Peterson, 1991; Aydin, 2000; Odling et al., 2004), the dynamics and size of earthquake ruptures (Aki, 1989; Harris and Day, 1999; Harris et al., 1999; Wesnousky, 2006; Shaw and Dieterich, 2007), the spatial and temporal evolution of earthquakes (Dewey, 1976; Toksöz et al., 1979; Stein et al., 1997), and growth and scaling of faults (de Joussineau and Aydin, 2009; Scholz, 2002).

One of the fault scaling relationships concerns fault length (L) to maximum fault slip or displacement (D). Various studies of mostly normal faults (Watterson, 1986; Walsh and Watterson, 1987; Cowie and Scholz, 1992; Schlische et al., 1996; Scholz, 2002) concluded that the length–slip relationship has the form, $L = D^n$, where n was proposed to be between 1 and 2.

Neighboring segments of strike-slip faults are separated by steps (Fig. 1a). These steps have self-similar geometry regardless of the sense of stepping and sense of shearing (Aydin and Schultz, 1990; Aydin and Nur, 1982). However, the failure modes and the distribution of the shearing-related structures may be different from one sense of step to another depending on loading, stress perturbations, rheology, and the geometry of initial pre-faulting discontinuities (Kim et al., 2004; Myers and Aydin, 2004; Peacock and Sanderson, 1991, 1995; Burgmann and Pollard, 1994; Sibson, 1986; Gamond, 1983; Rispoli, 1981).

A data set collected by Wesnousky (1988) from crustal-scale strike-slip faults suggests that the number of steps per kilometer along strike-slip faults decreases as fault slip increases. Although it

* Corresponding author.
E-mail address: aydin@stanford.edu (A. Aydin).

0191-8141/$ – see front matter © 2009 Elsevier Ltd. All rights reserved.
doi:10.1016/j.jsg.2009.11.007

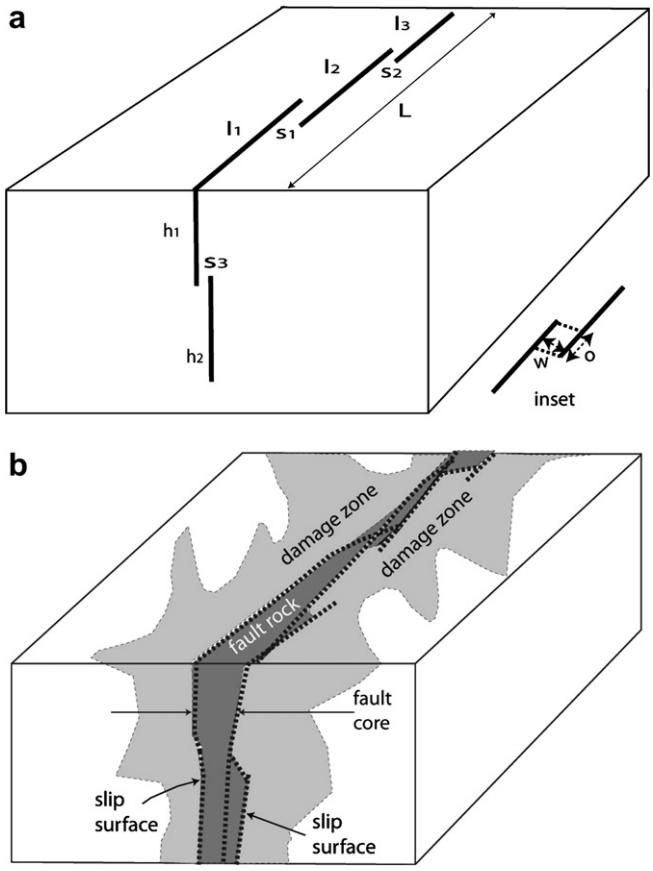

Fig. 1. Idealized diagrams showing: (a) segmentation along strike-slip faults and their segment lengths, heights and step numbers. Overlaps (or step lengths) and step widths (or fault separations) are also shown in inset. (b) Internal architecture of a strike-slip fault showing fault core, which includes fault rock and slip surfaces, and the surrounding damage zone.

is difficult to define uncertainty regarding the fault dimensions measured from published geologic and seismologic maps, recent experimental (Otsuki and Dilov, 2005) and site-specific field data from the same tectonic region and lithology and similar resolution (de Joussineau and Aydin, 2009) appear to confirm this trend. It is also interesting to note that larger size of steps is associated with faults having larger maximum slip magnitudes (Aydin and Nur, 1982; de Joussineau and Aydin; 2009), possibly related to the ability of fault slip to jump from one fault segment to next over the fault steps between them (Shaw and Dieterich, 2007; Harris and Day, 1999; Harris et al., 1999).

The fault length-slip, and step count per kilometer length relationships, regardless of their exact form, imply that faults, like other types of geological structures having different senses of displacement discontinuity, start small in length and grow larger in time and space. As faults grow longer, they are able to interact with the neighboring faults at greater distances. Consequently, faults extend their lengths by linkage and coalescence of smaller segments through fault steps in order to accommodate larger amount of slip (Segall and Pollard, 1983; Martel et al., 1988; Martel, 1990; Peacock and Sanderson, 1995; Cartwright et al., 1995; Dawers and Anders, 1995; Pachell and Evans, 2002; Scholz, 2002; Myers and Aydin, 2004; de Joussineau and Aydin, 2009). It follows that the fault length-maximum fault slip plots for faults which grew by linkage and coalescence for any single fault zone is not actually continuous but rather have sharp "jumps" coinciding with large increases in lengths at the merger of neighboring segments and "flats" corresponding to the time span between the consecutive merger instances, in which fault lengths stay nearly constant while fault slips increase to the limiting length/slip ratio (Cartwright et al., 1995)

Another type of fault scaling relationship illuminates how fault zones become wider as they grow (Fig. 1b). Field data (Hull, 1988; Robertson, 1983; Knott et al., 1996) and theoretical considerations (Scholz, 2002) suggest that the width or thickness of faults increases linearly with fault slip. Agosta and Aydin (2006) and de Joussineau and Aydin (2007) proposed that fault rock zones grow or widen perpendicular to their trend at the expense of highly fractured inner damage zone via cataclastic deformation. This widening is also influenced by the width of the steps along faults (Kim et al., 2004; Childs et al., 2009), which are precursors of fault cores.

An important consequence of lengthening of faults by linkage and coalescence is that larger magnitude of slip takes place in merged or composite segments which tend to straighten the overall through-going fault trace with respect to the earlier segmented or discontinuous trace. This process, which appears to be a second order shear localization phenomenon immediately after the fault zone attains the next composite configuration, is referred to as through-going faulting, fault straightening, and fault zone simplification (Cox and Scholz, 1988; Reches and Lockner, 1994; Le Pichon et al., 2001; Scholz, 2002; Ben-Zion and Sammis, 2003).

As this short introductory account indicates, the discontinuous geometry of strike-slip faults, their segmentation, the geometry and scaling of the segments and steps, and their impact on earthquake rupture, fluid flow and mineralization have attracted considerable interest in the literature. However, aside from a number of papers addressing the stress state between neighboring faults and the type and orientation of the linkage structure (Segall and Pollard, 1980; Pollard and Segall, 1987; Du and Aydin, 1993; Crider and Pollard, 1998; De Bremaecker and Ferris, 2004), very little attention has been paid to quantification of the elastic parameters leading to the growth of the fault dimensions. To this end, only a handful of studies address these criteria. The first group of these papers includes those dealing with calculation of the critical damage parameters at fault steps in terms of strain invariants (Lyakhovsky and Ben-Zion, in review; Lyakhovsky et al., 1997). The second category is rather empirical and is based on a field survey of normal faults and subsequent analysis of displacement-segment separation ratio to define those fields with unlinked and linked configurations (Soliva and Benedicto, 2004). A large number of publications deal with calculating effective moduli of fractured materials (Lockner and Madden, 1991; Sayers and Kachanov, 1991; Berryman and Grechka, 2006; Grechka and Kachanov, 2006; Berryman, 2008; Griffith et al., 2009). However, these do not address directly the subject of the actual fault growth and the related problems.

In this paper, we present natural and idealized fracture patterns around faults and within fault steps from the Valley of Fire State Park, Nevada, and use effective medium theory to investigate how rocks around and between fault segments weaken by faulting-related fractures and, consequently, how these intensely fractured rock masses may facilitate the growth of fault dimensions. Effective medium theory (sometimes called mixture theory, averaging, up-scaling or homogenization) is a collection of analytical methods designed to capture average properties and behaviors of very complex and heterogeneous media (Berryman, 2008). These methods have been applied to almost any type of complex system and physical property, but they tend to work best for quasi-static behaviors such as those considered in the present paper. A related paper (Berryman and Aydin, in press) dealing with the methodology in more detail for calculating effective moduli of fractured media will be presented somewhere else.

2. Geological background

For more than a decade, one of us (A.A.) and his students have been studying the initiation, interaction and growth of brittle, primarily strike-slip faults in the Jurassic eolian Aztec Sandstone with excellent exposures in the Valley of Fire State Park, about 60 km northeast of Las Vegas, Nevada (Fig. 2) (Çakir and Aydin, 1994; Flodin et al., 2005; Myers and Aydin, 2004; Flodin and Aydin, 2004; de Joussineau and Aydin, 2007, 2009; de Joussineau et al., 2007). We have documented that these Cenozoic faults (Bohannon, 1983) with both left- and right-lateral offsets ranging from a few millimeters to a few kilometers initiated from a system of joint zones by shearing of the joints, formation of new splay fractures and their subsequent shearing. By mapping of strike-slip faults with increasing magnitude of slip, the mechanism of fault growth was established to be the linkage and coalescence of initially sheared joint zones and of fault segments at progressively greater scales (Myers and Aydin, 2004; Flodin and Aydin, 2004; de Joussineau and Aydin, 2007). It was also concluded that the pattern and orientations of these faults within the Valley of Fire and the surrounding area are reminiscent of the large size strike-slip faults in the southeastern Basin and Range province (Çakir et al., 1998). The conceptual models and the field data in the next two sections ultimately rest upon these early publications as well as some new data and synthesis.

3. Conceptual models

Fig. 1a is an idealized diagram illustrating fundamental geometric attributes of strike-slip faults. Along-strike view shows segments with various lengths (l_1,l_2,…,l_n), which include the slip vector direction by definition. Hence, identifying segments assures a basis for determining mean and maximum segment lengths. This view also shows discontinuities along the trace length in the form of steps (s_1,s_2,…,s_{n-1}) with overlaps (o_1,o_2,…,o_{n-1}) and widths (w_1,w_2,…,w_{n-1}) or separations (Fig. 1a inset). These parameters provide the bases for calculating the number of steps per length, and the size of the steps along a given strike-slip fault.

Down-dip view also includes segments with steps. We will not consider down-dip segmentation and steps because these steps do not provide much resistance to strike-slip motion due to the slip vector being horizontal and therefore the linkage is relatively simple. In vertically anisotropic lithologies, the problem becomes more complex by the presence of inelastic rocks such as shale, which is out of the scope of this paper.

Fig. 1b shows a detailed view of fault zone architecture with a fault core, made up of fault rock and slip surfaces. Fault rock is the product of fragmentation and cataclasis when a highly fractured rock is disaggregated, fracture-bounded blocks rotate and translate and grains crush. Slip surfaces are discrete structures that accommodate shear displacement along polished and striated surfaces which usually run through, or occur adjacent to, the fault rock. Fault cores are flanked on both sides by a damage zone which includes a complex fracture system of splay joints and sheared splay joints of various generations. We note that, as depicted in the diagram, the distributions of fault rock and damage zone are highly irregular. The diagram in Fig. 1b also illustrates the notion that one of the major slip surfaces within the fault core may be continuous from one end to the other, which is meant to represent a through-going fault surface, and accommodates a large portion of the total slip across the fault zone.

4. Field data

Here, we focus on dimensional attributes and growth processes of a network of strike-slip faults exposed in the Aztec Sandstone cropping out in the Valley of Fire Sate Park and its surroundings (Fig. 2). Although the geometric and mechanical properties of the strike-slip faults at this location appear to be similar to those strike-slip faults from different regions (de Joussineau and Aydin, 2009) as summarized in Section 1, we restrict our statistical and conceptual models to the cases that we studied in some detail at the Valley of Fire State Park for two reasons. One is that the mechanisms of fault initiation and growth are well known and the precision of measurements is very good and fairly uniform in a wide range of scales.

4.1. Fault segment length, step number and dimensions, and fault width

Data from about 20 well-exposed faults in the study area show that the mean segment length increases with the maximum fault

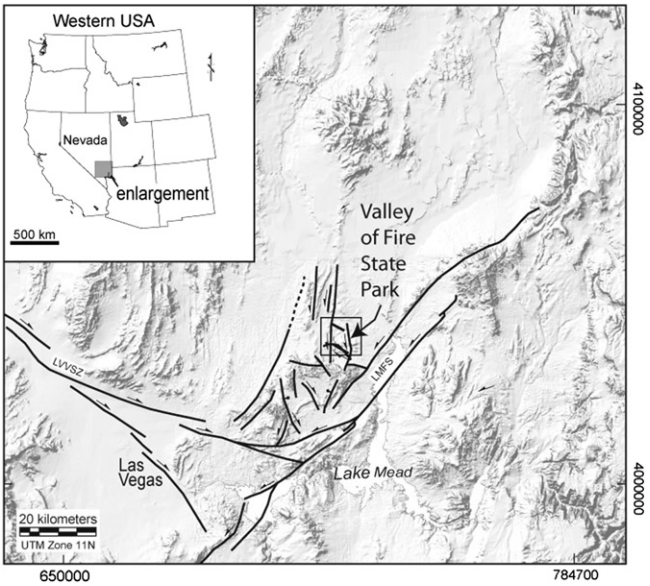

Fig. 2. Location and simplified map of the faults of Cenozoic age in the Valley of Fire region of southern Nevada. Heavy lines are faults. Arrows indicate predominant sense of slip. LMFS, Lake Mead Fault System; LVVSZ, Las Vegas Valley Shear Zone. Rectangle marks the location of the Valley of Fire State Park.

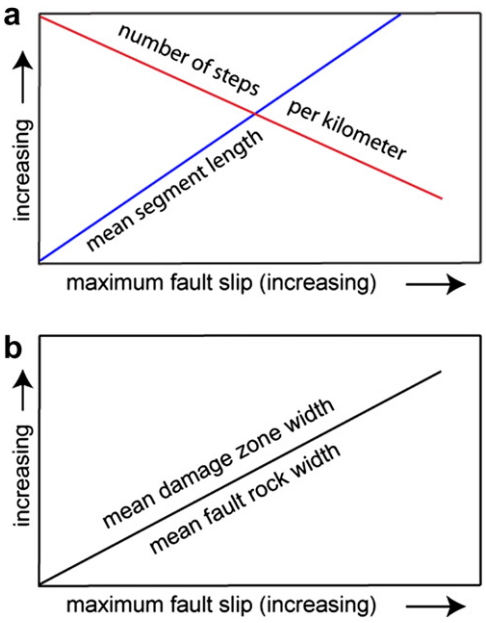

Fig. 3. Idealized diagrams summarizing general trends of (a) mean segment length and number of steps per kilometer, and (b) mean fault rock and mean damage zones widths as the maximum fault slip increases.

slip (de Joussineau and Aydin, 2009) as idealized in Fig. 3a. Here, we use a simple idealized trend because the exact nature of the relationship is not the focus. Data collected from the same faults also show that the number of steps per kilometer decreases as a function of the maximum fault slip. Stating this result in a simpler way; when n number of segments is reduced to $n-1$ segments by linkage of the two neighboring segments, then, $n-1$ number of steps will be reduced down to $n-2$ steps by destruction of one of the steps.

The damage zone and fault rock widths increase with increasing fault slip (de Joussineau and Aydin, 2007, 2009; Flodin et al., 2005; Myers and Aydin, 2004). These relationships are not locally smooth, but regardless of the actual forms, can be idealized as shown in Fig. 3b. These trends are more meaningful for considering either mean or maximum widths versus maximum slip values. For example, the damage zone widths are controlled primarily by the location, angle and length of the splay fractures (de Joussineau et al., 2007) whose distribution about the fault may be highly nonuniform.

The nature of fracturing at small fault steps can be characterized as initial splay fracturing in response to shearing of the echelon joints (Fig. 4a) and then shearing of the 1st generation of splay fractures and formation of a 2nd generation splay fractures that connect the sheared 1st generation splay fractures (Fig. 4b). The intersection angle between the sheared joints and the 1st generation splay fractures varies from about 15° to 85° with an average value of about 19° for isolated sheared joints, and about 50° for subparallel interacting sheared joints (Fig. 5a,b and Table 1a).

Terminal areas of a fault zone generally reflect the incipient stages of fault development. In this regard, Fig. 6 shows a portion of a fault zone that has ~65 cm maximum observable right-lateral slip elucidating the transition from an echelon sheared-joints array to a through-going fault formation. Similar to the cases shown in Fig. 4, shearing of the initial joint system resulted in splay fracturing and continued shearing facilitated the formation of multiple sets of sequential splays localizing into discontinuous pockets of high density fractures, and, in places, fragmentation zones. The incipient short slip surfaces eventually go through these pockets of weakened rock at fault steps.

The photographs and maps in Fig. 7a,b show a well-exposed fault of about 14 m left-lateral slip, which displays several characteristic architectural elements common to all strike-slip faults in the study area: Fault rock, slip surfaces, and damage zone. Fig. 7a shows domains of different deformation zones and of fracture densities, which allow one to see a simpler picture of elongated, noncolinear bodies of the fault rock and the adjacent areas of high fracture density. Fig. 7a,b also shows slip surfaces in various orientations and sizes, one of which is continuous from one end of the mapped area to the other going through the elongated bodies of fault rock. There are also short slip surfaces terminating at an acute angle to the rectilinear strings of fault rock (Fig. 7b). We interpret these diagonal short slip surfaces as relics of the initial sheared joints and the high

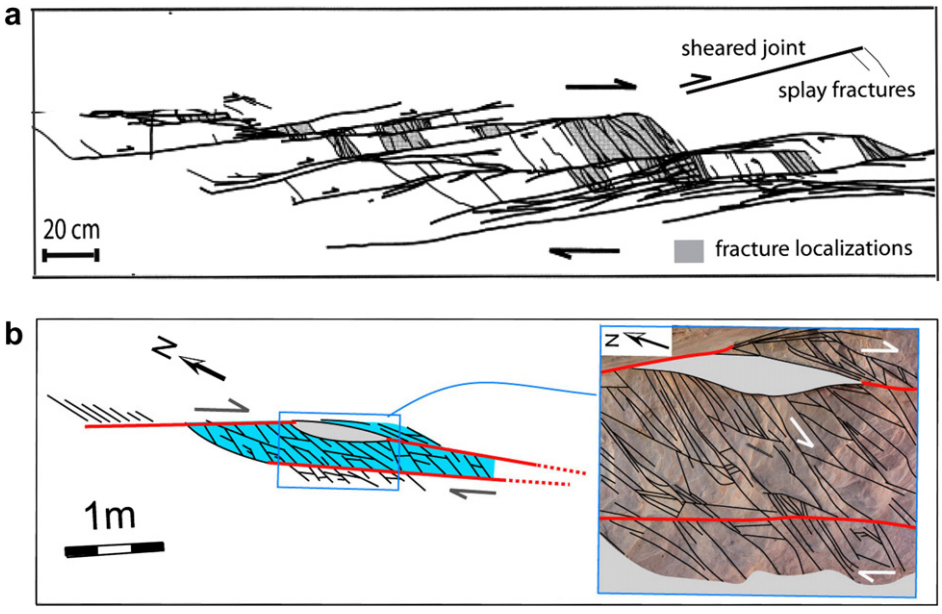

Fig. 4. (a) Incipient right-lateral shearing (~2 cm) of a series of echelon joints with right steps. Splay fractures at high-angle to the sheared joints are localized near the tips of the segments at the steps. From Myers and Aydin (2004). (b) Two sets of splay fractures at and around a right step along a strike-slip fault with about 80 cm right-lateral slip. The two sets have a range of intersection angles from 30° to 60°. From de Joussineau and Aydin (2009).

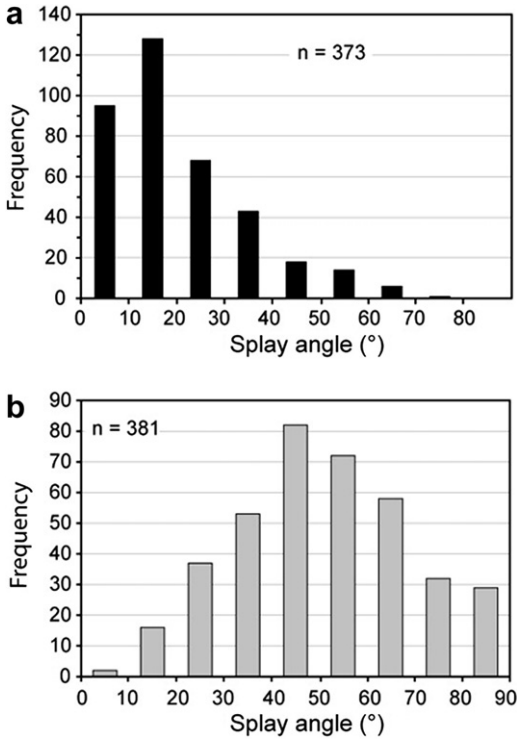

Fig. 5. Histograms showing the distribution of the intersection angles between faults and their splay fractures (splay angles) for more than 750 measurements. (a) For isolated faults, and (b) for closely spaced, interacting subparallel faults. From de Joussineau et al. (2007).

intensity fracture zones, to a large extent, fracture localization between these sheared joints. Then, the fault rock and the associated slip surfaces subparallel to the fault core represent the architecture of a new progression in fault growth with a through-going fault core and slip surface representing the latest linkage and coalescence structure, for this portion of the fault. This elucidation makes an important point that any given stage of progressive faulting includes overprinted patterns of fault zone elements, which poses a major challenge in predicting a fault's architecture without sufficient information for its deformation history.

The 14 m fault described above also displays characteristics of its damage zone. Fig. 8a,b shows photos and details of fractures on one side of this fault. The fault core and the inner and outer damage zones are shown in Fig. 8a. The details of the inner damage zone are shown in Fig. 8b. Here, several generations of splay fractures are identified based on their abutting relationships and marked by different color codes. The younger ones fill in between the echelon sheared joints of the initial stage (de Joussineau and Aydin, 2007). Fig. 8c shows a photo and a detailed map of fine- and coarse-grained fault rocks and major through-going slip surfaces along a strike-slip fault with about ~25 m left-lateral slip. Some of the earlier fractures within the coarse-grained fault rock can still be identified (dotted lines). Also important to point out are the triangular pockets of fine-grained fault rock protruding into the damage zone on the left hand side of the fault core, where the fracture intensity appears to be high. The triangular zones between one of the main slip surfaces and sheared splay fractures (one marked in the map as "x") are known to be the location of higher fracture concentrations based on observations at other locations with similar geometric settings (Flodin and Aydin, 2004).

A conceptual model depicting linkage and coalescence of fault segments or strands which result in longer segment lengths, reduced number of fault steps per kilometer, and wider damage zones and fault core with increasing fault slip is shown in Fig. 9. In a simple way, the model illustrates how strike-slip faults grow via an interrelated series of processes including splay fracturing, shearing of splay fractures, segment linkage, and formation of through-going slip surfaces in a hierarchical manner. Progressive lengthening of the linked segments, in turn, drives splay fractures to farther distances from the main body of the fault and thus increases the size of potential steps and eventually the widths of fault cores and fault damage zones.

The types of field data crucial for the fault growth are the density or spacing of the fault-related fractures as well as their patterns. In the study area, a vast amount of data is available for the distribution of the fault-related fractures (de Joussineau and Aydin, 2007, 2009; de Joussineau et al., 2007; Flodin and Aydin, 2004; Myers, 1999). Fig. 10a displays one of these for the left-lateral fault

Table 1
(a) The average fracture intersection angles for isolated faults and their splays (19°), and for closely spaced interacting subparallel faults and their splays (50°). From de Joussineau et al. (2007). (b) The spacing range defined by the best fit line to the smallest end of the spacing distribution of the fault-related fractures in the study area. From de Joussineau and Aydin (2007). The spacing values obtained by this method are between ~1 and 5 cm with the largest concentration between 1 and 2 cm (see inset 1). The angular differences between the scanline and fault-related fractures for 14 m fault (inset 2 in which the bins represent intervals of 0–9, 10–19, etc.). More than 75% of the fractures make angles larger than 50° to the scanline (see the diagram within inset 2 for designing the angle between scanline and a fracture set (α) and the true and apparent spacing (S_t and S_a, respectively)). This requires a maximum correction factor of about 0.77.

a

Pattern type	Average splay angle
Isolated/single fault	19°
Interacting faults	50°

Inset 1

b

Fault	Spacing range (cm)
80 cm	1.5–18
8 m	2.0–39
14 m	2.0–51
80 m	1.4–110
Mixed	
Scanline #1	2.0–52
Scanline #2	0.9–14
Scanline #3	5.0–38

Inset 2

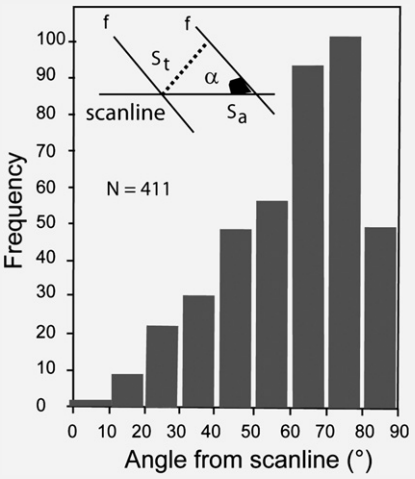

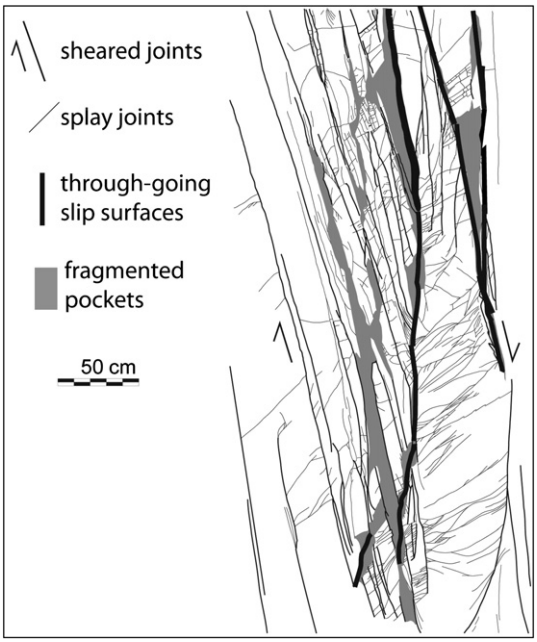

Fig. 6. Detailed map of the end of a small shear zone of about 65 cm observable maximum right-lateral slip showing a set of slightly sheared and highly overlapped echelon joints and sheared joints with many splay joints at high-angle to the sheared joints. Gray shading marks narrow pockets of fragmentation and thick lines show incipient through-going slip surfaces orientated at a small-angle to the sheared initial echelon joints. Slightly revised from Davatzes and Aydin (2004).

with 14 m slip referred to earlier in this manuscript (see Figs. 7 and 8). The spacing distribution for the fault-related fractures for this fault has been determined along 8 scanlines perpendicular to the fault trace in intervals about 2–6 m recording the distance, orientation and length of the fractures with a resolution of 0.5 cm. The spacing has been calculated as the distance between consecutive fractures. Of interest here is the spacing distribution on the smaller end of the spectrum identified by the linear trend in the spacing distribution plot which defines a range of spacing values from 2 to 51 cm (see Fig. 10a). Fig. 10b shows the fracture spacing distribution obtained from a single scanline across many faults with aggregate slip on the order of a few hundreds of meters. Here the range of the smallest linear spacing trend is 5–38 cm. In both cases, we focus on the smallest ends of the ranges, 2 cm in Fig. 10a and 5 cm in Fig. 10b) which represent the smallest fracture spacing for a statistically significant number of data points measured near the fault cores. Similarly, in Table 1b, the spacing ranges defined by the linear fits to the smallest slopes in the distribution of data, and the corresponding minimum spacing values, for three other faults and two additional scanlines across a number of faults are given. As shown in the histogram summary (inset 1) a majority of the minimum spacing values falls between 1 and 2 cm. Considering the minimum measurable spacing was 0.5 cm, these numbers are well above the minimum resolvable spacing.

5. Analysis using effective medium models

The premise of this study is that a certain degree of high intensity fracturing at fault steps and fault damage zones weakens the rock masses thereby facilitating fault lengthening through linkage and coalescence of neighboring segments and fault zone widening by incorporation of the fractured and fragmented material into the fault rock via a cataclastic process.

Next, we will use effective medium models to investigate the degradation of the strength and reduction of resistance to cataclastic deformation, which presumably pave the way for the setting of through-going faults. Given the complexity of the

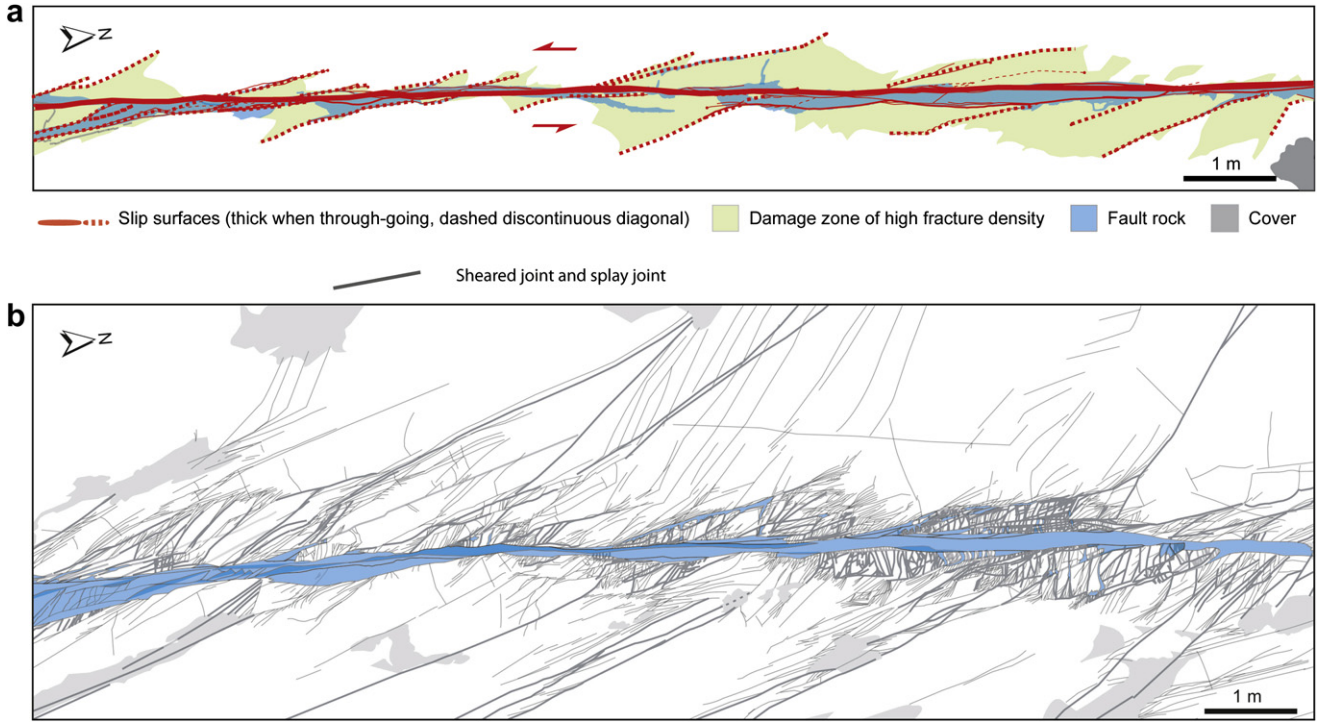

Fig. 7. (a and b). Detailed maps of a strike-slip fault with about 14 m left-lateral slip. (b) shows the orientations, lengths, and intersections of damage zone fractures (splay joints and sheared splay joints) around the fault core (Myers and Aydin, 2004) whereas (a) shows a new reinterpreted version of the same fault architecture in which noncolinear pockets of fault rocks and highly fractured domains of occasionally fragmented damage zone are delineated in the field. One through-going slip surface (thick solid line) and several short slip surfaces (dotted lines) diagonal to the through-going slip surface are highlighted. The geometry and distribution of many of short diagonal slip surfaces resemble the initial echelon sheared joints observed along faults with smaller slip in the area. The original map by R. Myers (1999); the present version was revised from Davatzes and Aydin (2004).

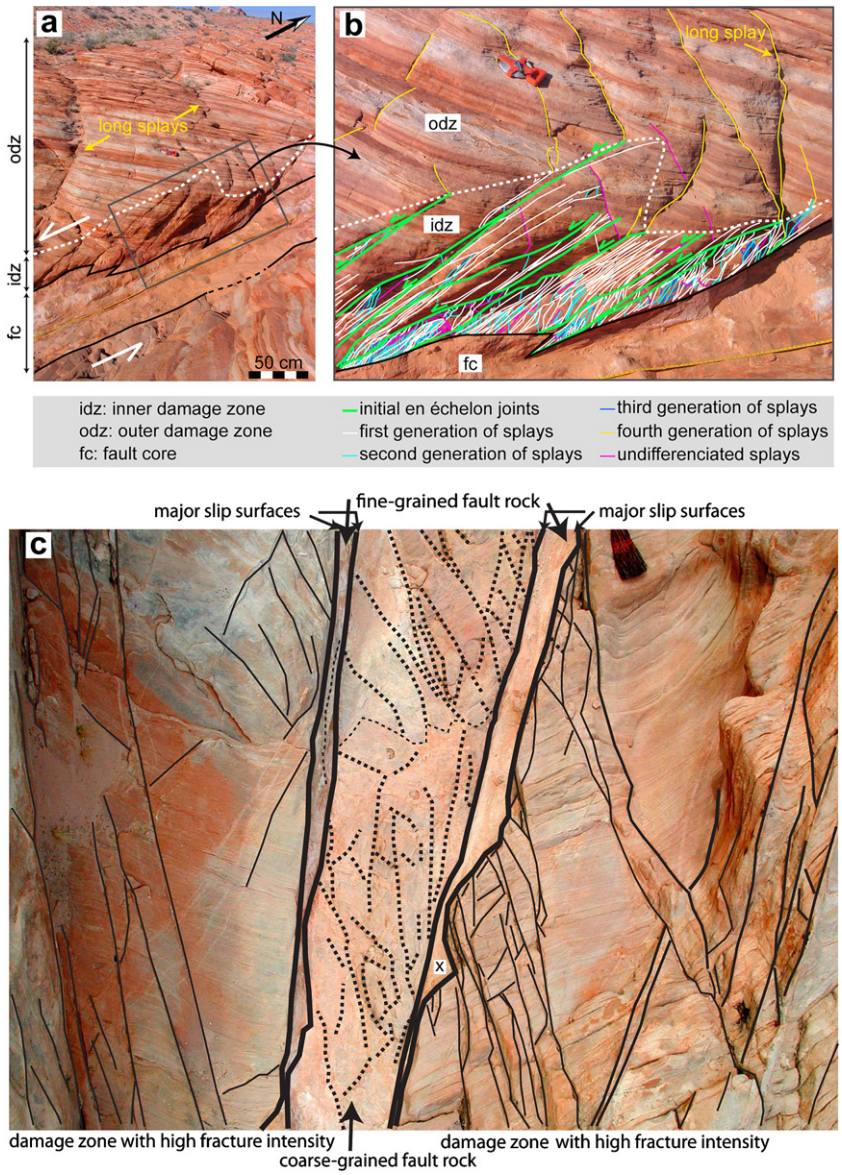

Fig. 8. Damage zone characteristics around the strike-slip fault with ~14 m left-lateral slip. (a) Two fractured domains were distinguished: The inner damage zone of high fracture density right next to the fault core; and the outer damage zone of significantly lower fracture density. (b) A detailed map of the inner damage zone shows that several generations of splay fractures (marked by different color codes) fill in between the echelon sheared joints of the initial stage. (a,b) From de Joussineau and Aydin (2007). (c) Detail map showing fine- and coarse-grained fault rock and major through-going slip surfaces along a left-lateral fault with about 25 m left-lateral slip. Some of the earlier fractures within the coarse-grained fault rock can still be identified (dotted lines). Also important to point out triangular pockets of fine-grained fault rock protruding into the damage zone in some locations on the left hand side of the fault core, where the fracture intensity is the highest.

fractures around faults, the problem is obviously rather difficult and, at this stage, further simplification is desirable for applications to an effective medium theory. We first idealize the common fracture patterns in terms of their orientation-intersection angle, length, and density (Fig. 11a). We then study parametrically the effective elastic moduli of such a configuration as a function of fracture density for each idealized fracture pattern defined by the angle between fracture sets in order to assess the degree of degradations in the moduli values as the fracture density increases. The details of the effective medium theory that we shall employ have been recently described by Berryman and Aydin (in press) and is based on the earlier work by Backus (1962), Schoenberg and Muir (1989), and Berryman and Grechka (2006).

Fig. 11a shows an idealized fracture network which is consistent in principle with the sequential formation of two fracture sets and their ultimate pattern, the examples of which can be seen in Figs. 4, 6, 7, and 8. Here the lengths (l) of the fractures, the density (ρ) or spacing (s) of the fractures, and angle (Φ_F) between the two sets of fractures characterize the pattern in a layer with a thickness, h.

One of the most commonly used fracture density concepts goes back to Bristow (1960) and Budiansky and O'Connell (1976). For a set of rectangular flat (or a ribbon-shaped) fractures, which is the most pertinent to physical properties of fractured media such as resistivity, fluid flow, and elasticity, is

$$\rho = nh^2l \tag{1}$$

where $n = N/V$, with N and V being the number of fractures and the rock volume, respectively. The volume, V is equal to lhs where l, h, and s are average fracture length, height, and spacing, respectively. Taking t as the average fracture thickness or fracture aperture, the porosity of a system of rectangular flat fractures with an average

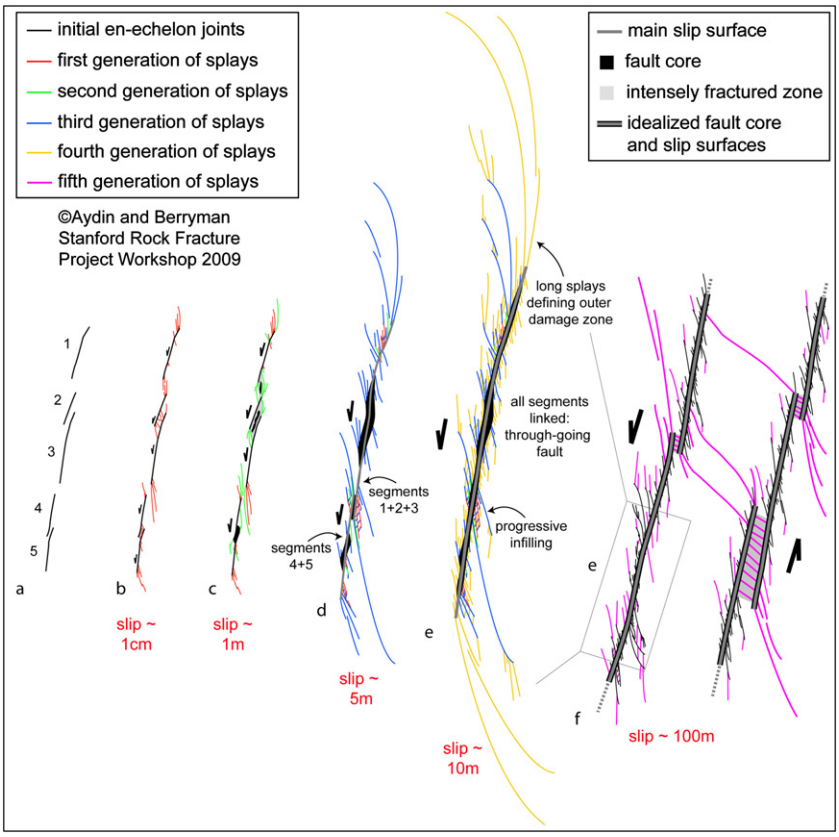

Fig. 9. Conceptual model showing linkage and coalescence of fault segments or strands which result in longer segment lengths, reduced number of fault steps, larger step sizes, and wider damage zones and fault rock zones with increasing fault slip. From de Joussineau and Aydin (2007).

spacing value, s, is defined as a fraction of the spacing distance occupied by the pores:

$$\varphi = lht/V = t/s \tag{2}$$

Then, the fracture density is given as

$$\rho = h/t \sim h/s \tag{3}$$

Based on Eqs. (2) and (3), we find that the fracture density as defined here is proportional to height or bed thickness over spacing and is dimensionless. The fracture density of, for example, 1.0, corresponds to a commonly observed average spacing for one set of opening mode fractures in a bed, for which the average spacing, s, scales with the bed thickness, h, for well-developed fracture systems (Wu and Pollard, 1995; Bai and Pollard, 2000). Thus, for a bed thickness of 5 cm, the average spacing is 5 cm. For two sets of overlapping fracture systems of equal density in a bed, the value for the density approaches 2.0, and the average spacing is $h/2$. For a bed of 5 cm thick, the equivalent spacing for the two overlapping sets is 2.5 cm.

5.1. Compliance matrix and the corresponding Young's and shear moduli components

The quasi-static equation of elasticity using Voigt notation is (Nye, 1985; Pollard and Fletcher, 2005):

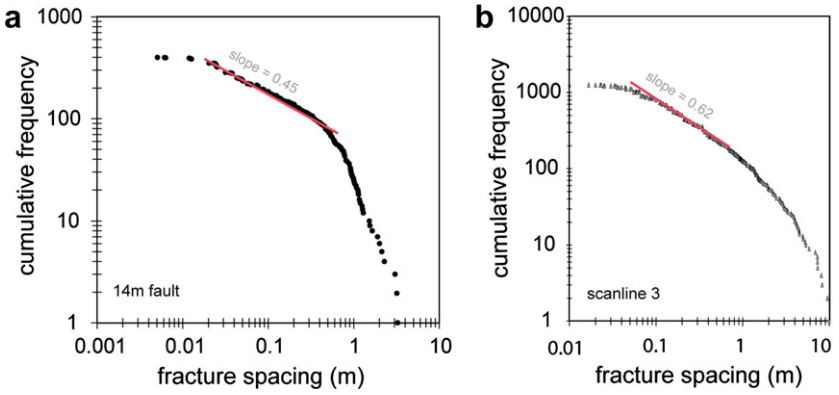

Fig. 10. Fracture spacing distributions: (a) for the 14 m fault and (b) across an area which included many faults with an aggregate slip of a few hundred meters. The line fits to the data at the smallest ends of the spacing range are also shown. The smallest spacings defined by these linear trends are taken as the critical values below which the systems are thought to be unstable. Slightly changed from de Joussineau and Aydin (2007).

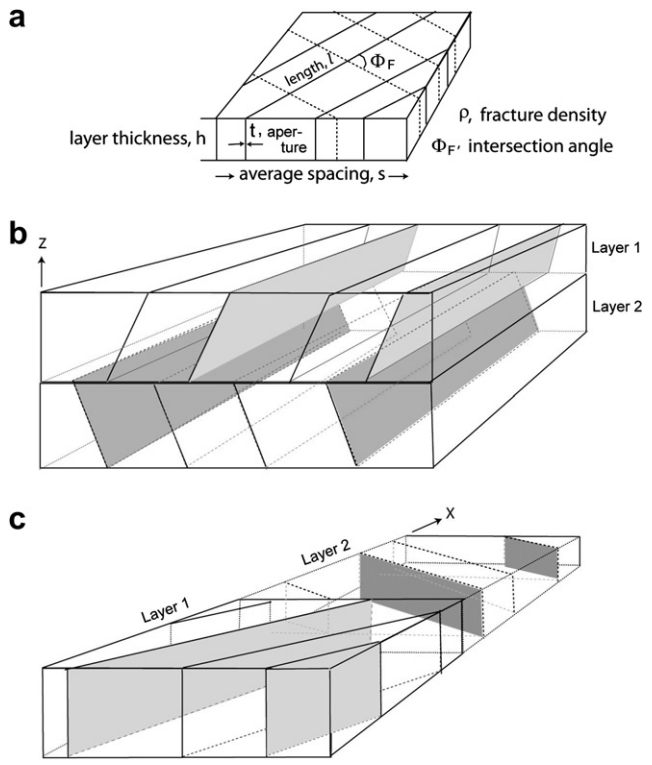

Fig. 11. (a) A simplified and idealized fracture pattern at fault steps and within inner damage zones. The pattern is defined by the angle (Φ_F) between the two fracture sets and lengths (l) and density (ρ) of the fracture systems. Fracture density is proportional to the ratio of layer thickness or fracture height (h) to average spacing (s). (b,c) Block diagrams showing the procedure to represent layers with each fracture set and the configurations of the layers for averaging the effective properties in z- and x-directions or 3- and 1-directions, respectively. The block diagrams represent stacking up layers vertically in z-direction ((b) sandwich configuration) and arranging the layers side by side in x-direction ((c) contiguous configuration).

$$\begin{pmatrix} \varepsilon_{11} \\ \varepsilon_{22} \\ \varepsilon_{33} \\ \varepsilon_{23} \\ \varepsilon_{31} \\ \varepsilon_{12} \end{pmatrix} = \begin{pmatrix} S_{11} & S_{12} & S_{13} & S_{14} & S_{15} & S_{16} \\ S_{21} & S_{22} & S_{23} & S_{24} & S_{25} & S_{26} \\ S_{31} & S_{32} & S_{33} & S_{34} & S_{35} & S_{36} \\ S_{41} & S_{42} & S_{43} & S_{54} & S_{45} & S_{46} \\ S_{51} & S_{52} & S_{53} & S_{54} & S_{55} & S_{56} \\ S_{61} & S_{62} & S_{63} & S_{64} & S_{65} & S_{66} \end{pmatrix} \begin{pmatrix} \sigma_{11} \\ \sigma_{22} \\ \sigma_{33} \\ \sigma_{23} \\ \sigma_{31} \\ \sigma_{12} \end{pmatrix} \tag{4}$$

where ε and σ are the six independent components of strain and stress, respectively, and S is the symmetric 6-by-6 compliance matrix. The numbers 1, 2, 3 always indicate Cartesian axes (say, x, y, z respectively). Elastic extension in the x- or 1-direction is denoted by ε_{11}, etc., while a shearing (torsion or twisting) strain around the x- or 1-axis is represented by ε_{23}, etc. Similarly, the normal stress or tension in the x-direction is σ_{11}, and the shear stress around the x-axis is symbolized by σ_{23}, etc.

For any system, the full compliance matrix (Eq. (4)), or its inverse, the stiffness matrix, has six eigenvectors, each of which is a 1×6 matrix and is associated with a scalar eigenvalue. If S is the matrix, v is the eigenvector, and c is the eigenvalue, then by definition $Sv = cv$. This means that when matrix S is multiplied by vector v, the result is a vector proportional to v, and the constant of proportionality is the eigenvalue c. There are always 6 distinct eigenvectors. However, eigenvalues may or may not all be distinct. For an isotropic system, five of these eigenvalues are for shearing modes and one is for pure compression/tension mode. Of the five shearing modes, three are the independent torsional or twisting motions and/or the corresponding stresses; for example, in an isotropic system, ε_{23}, couples simply to σ_{23}, while all the off--diagonal compliances and/or stiffnesses involving subscripts 4, 5, 6 vanish identically. Two other types of shear modes are eigenmodes for an isotropic system; for example, when $\sigma_{22} = -\sigma_{11}$, we have a comparable "push-pull" or "pure shear" mode resulting in the eigen-response $\varepsilon_{22} = -\varepsilon_{11}$ for the strain. For the isotropic case, there are three distinct versions of these pure shear behaviors that give analogous results, but for nonisotropic systems usually only one of these will actually be an eigenmode – the most common example of this behavior being for transversely isotropic systems.

In the presence of a set of perfectly parallel fractures in an otherwise isotropic elastic medium, the elastic matrix becomes transversely isotropic. The plane of the parallel fractures is the plane of symmetry, and the direction perpendicular to this plane is the axis of symmetry. Elastic behavior strictly within the plane of symmetry (i.e., two-dimensional behavior in this plane) remains isotropic, which is the origin of the term "transverse isotropy" – this type of isotropic behavior thus occurring transversely to the axis of symmetry.

When analyzing such systems in three-dimensional space, it is common to choose the axis of symmetry to coincide with one of the spatial axes, x, y, and z, or 1, 2, and 3, respectively. This choice makes no difference to the final results but makes some difference to the level of difficulty in obtaining those results. In particular, making a good choice of axes can simplify the matrix of elastic coefficients somewhat, so that, for a set of parallel fractures, we have a compliance matrix in the Voigt (Nye, 1985) 6×6 matrix form of the elastic tensor notation:

$$S = \begin{pmatrix} \frac{1}{E_{11}} & \frac{-\nu_{12}}{E_{11}} & \frac{-\nu_{13}}{E_{33}} & & & \\ \frac{-\nu_{12}}{E_{11}} & \frac{1}{E_{22}} & \frac{-\nu_{23}}{E_{33}} & & & \\ \frac{-\nu_{13}}{E_{33}} & \frac{-\nu_{23}}{E_{33}} & \frac{1}{E_{33}} & & & \\ & & & \frac{1}{G_{44}} & & \\ & & & & \frac{1}{G_{55}} & \\ & & & & & \frac{1}{G_{66}} \end{pmatrix} \tag{5}$$

Thus, for orthorhombic symmetry, the diagonal components of the matrix; the Young's moduli E_{11}, E_{22}, and E_{33} and the shear moduli G_{44}, G_{55}, and G_{66} are inversely related to these diagonal components. Note that the zero matrix elements were left blank in Eq. (5) for simplicity as is standard practice. A particular modulus that we call qGp, for quasi-pure shear mode is also calculated because it is likely to play a role in the failure of the systems we examine here, and it is well known in the geological sciences. The mode qGp is actually an eigenvector of the system considered, but its physical interpretation is not simple, because it is not exactly any one of the six standard modes of a simple elastic system pointed out earlier. However, its behavior is very close to that of a *pure shear* mode and that is why the term "quasi" is used here.

In calculating these components of the effective elastic moduli for a medium with Poisson's ratio of 0.4375 appropriate for sandstone, which has two fracture sets (Fig. 11a), we follow an approach based primarily on layer averaging methods of Backus (1962) and Schoenberg and Muir (1989). The details of the mathematical analysis of the effective properties of such a composite system are given by Berryman and Aydin (in press). Basically, two different layers each containing one set of fractures with the same density (ρ) but possibly differing distributions, are considered for the effective moduli calculations (Fig. 11b). After constructing one layer with one of the fracture sets, this layer is rotated in such a way that the combined fracture system will have the desired angle between the

two fracture sets. This is done by rotating each layer plus/minus one half of the angle between the two fracture sets. In this paper, we investigate cases where the angles between the two fracture sets (Φ_F) are 15°, 30°, 45° and 60°. The two layers are either stacked up, which we call "sandwich" configuration (Fig. 11b) or are placed side by side, which we call "contiguous" configuration (Fig. 11c). The former is used for averaging in the *z*- or 3-axis whereas the latter is used for averaging along the *x*- or 1-axis. Another side by side contiguous configuration similar to that in Fig. 11c is used for averaging along the *y*- or 2-direction. Both the contiguous and sandwich configurations represent interacting but not intersecting fracture arrays.

Fig. 12 shows the plots of the calculated effective moduli; (a) for the Young's moduli, (b) for the shear moduli, and (c) for the quasi-shear moduli for "pure shear" for each of the four different fracture configurations defined by the angle $\Phi_F = 15°$, 30°, 45°, and 60° and for a range of fracture densities from 0 to 0.2. This range of density is constrained by the availability (from previous work of Berryman and Grechka, 2006) of the fracture influence coefficients which are required for the effective property calculations. The results show that the E_{11} components of the Young's moduli for all four fracture configurations do not change at all (all four lines overlap along the top blue line in Fig. 12a) with increasing fracture density up to 0.2. This is because E_{11} corresponds to uniaxial loading in the *x*- or 1-direction and the changes of the angles and densities of fractures, as seen from this direction edge-on, make no difference on the effective moduli. The E_{22} and E_{33} components show systematic decrease for all configurations as the fracture densities increase. We note that the E_{22} for the configuration $\Phi_F = 60°$ and 45° experiences greater decreases for the range of densities than fracture sets with other intersection angles, whereas E_{33} shows greater decreases for configurations with smaller intersection angles, $\Phi_F = 15°$ and 30°. For example, the effective Young's modulus, E_{33}, corresponding to $\Phi_F = 15°$ at a fracture density of 0.2 shows about 34% reduction with respect to the value for a medium without any fractures ($\rho = 0$). We note that the plots for E_{22} and E_{33} have segments with different slopes indicating the nonlinear nature of the moduli variations as the density increases. Since the change of slope occurs at the fracture densities for which the calculations were performed, the change would have been smoother if more runs with intermediate fracture density values were performed.

The plots for the shear moduli components for the four fracture configurations are given in Fig. 12b. They all are nearly linear except one (G_{44}-shearing about the 1- or *x*-axis). G_{66} and G_{55} (shearing about the vertical 3- or *z*-axis and the 2- or *y*-axis, respectively) get monotonically weaker for the density range used. However, these moduli show the largest decreases for the fracture configurations 60° and 15°, respectively. The greatest decrease of the shear moduli occur in the G_{44} and G_{55} components (shearing about the 1- or *x*-axis and 2- or *y*-axis, respectively) corresponding to the fracture configurations with the lowest angle, $\Phi_F = 15°$. However, this decrease amounts to about 20% of the modulus for a medium without any fractures. The curves for G_{44} components have a crossover at a fracture density, ρ, between 0.1 and 0.15. This crossover is curious and remains to be investigated further.

Fig. 12c shows the variation in the effective quasi-shear modulus for pure shear (qGp) as being one of the special cases. This parameter shows a smaller variation of about 5% (with respect to the modulus for the no-fracture state) for $\Phi_F = 60°$ at the highest fracture density (0.2) used in the calculations.

5.2. Extrapolations

Because the concept of elasticity is based on energy storage in the elastic material/medium, there is an elastic conservative energy associated with the elastic system. Each eigenvalue is a measure of the elastic energy that can be stored in the system associated with its elastic matrix. Since these stored energies must be positive quantities, it follows that the eigenvalues themselves must all be positive. If any elastic eigenvalue for a system vanishes, then this means that it is impossible to store energy in this particular mode and that the strain of the system increases without additional stress if it is attempted to excite this mode. This condition defines a mechanical instability in the system. So it is reasonable to use this condition as one definition of mechanical system failure, and this is why we look for the appearance of such failed modes in our analysis of elastic system response. However, the vanishing values that we want lie outside the range of values in our plots. This is because, as pointed out earlier, the required fracture influence coefficients are not presently available for values outside of the range of densities considered here.

The ways in which the shear and quasi-shear moduli vary with increasing fracture density for each configuration in our models are nearly linear. This may warrant extrapolations using the last segment of the curves (for ρ between 0.1 and 0.2) to estimate the critical fracture densities corresponding to the vanishing values of shear moduli components. Hence, G_{55} and G_{44} plots for the intersection angle of 15° provide 0.9 for the critical density which is the upper bound for cataclastic failure. The qGp for pure shear gives the highest critical fracture density on the order of about 4, which implies that the failure will occur earlier due to a more significant weakening of the other elastic parameters. Although the Young's moduli curves showing greater decreases (E_{33}) appear to be highly nonlinear, again the last linear segments are used to approximate the densities corresponding to the vanishing value of this component. For these cases the critical values of densities are close to each other for each angular configuration being between 0.88 and 1.01. Just to provide a spacing value to which the JSG reader can relate to: These roughly correspond to a single set fracture spacing of about 5 cm for a 5 cm thick bed and 2.5 cm for two sets fracture spacing. However it is possible that cataclastic failure may occur at spacings lower than that for thinner layers and having the bedding interfaces fail as part of the fragmentation process which has not been considered in our analyses.

6. Discussion

The premise behind the present study is that the patterns of fractures at strike-slip fault steps and inner damage zones adjacent to fault rocks is complicated but can be simplified to represent the local damage fairly well. Due to high density of fractures, the mechanical properties of the rock masses at these locations are so altered that a new paradigm is required to analyze the conditions leading to the growth of faults by linkage of neighboring segments and by enlargement of fault rock into the adjacent inner damage zone through cataclastic deformation. The rationale for this premise is three fold. First, laboratory studies on porous granular rocks show a nearly linear trend between uniaxial strength and the Young's modulus (Palchik, 1999) and shear strength and the shear modulus (Holt et al., 1987). Second, there is a theoretical basis in linear elastic fracture mechanics (LEFM) for the fracture toughness being equal to the Young's modulus times the strain energy release rate. Thus, the toughness is proportional to the Young's modulus for a given fracture extension though in homogeneous elastic medium (Lawn and Wilshaw, 1975). Third, as has been referred to in this paper, the compliance matrix for anisotropic elastic materials links stresses to strains and should be crucial for determining the deformation of rocks including their yielding or failure.

Thus, this premise separates the present study from those using single linkage structure whether in opening, closing, or shearing

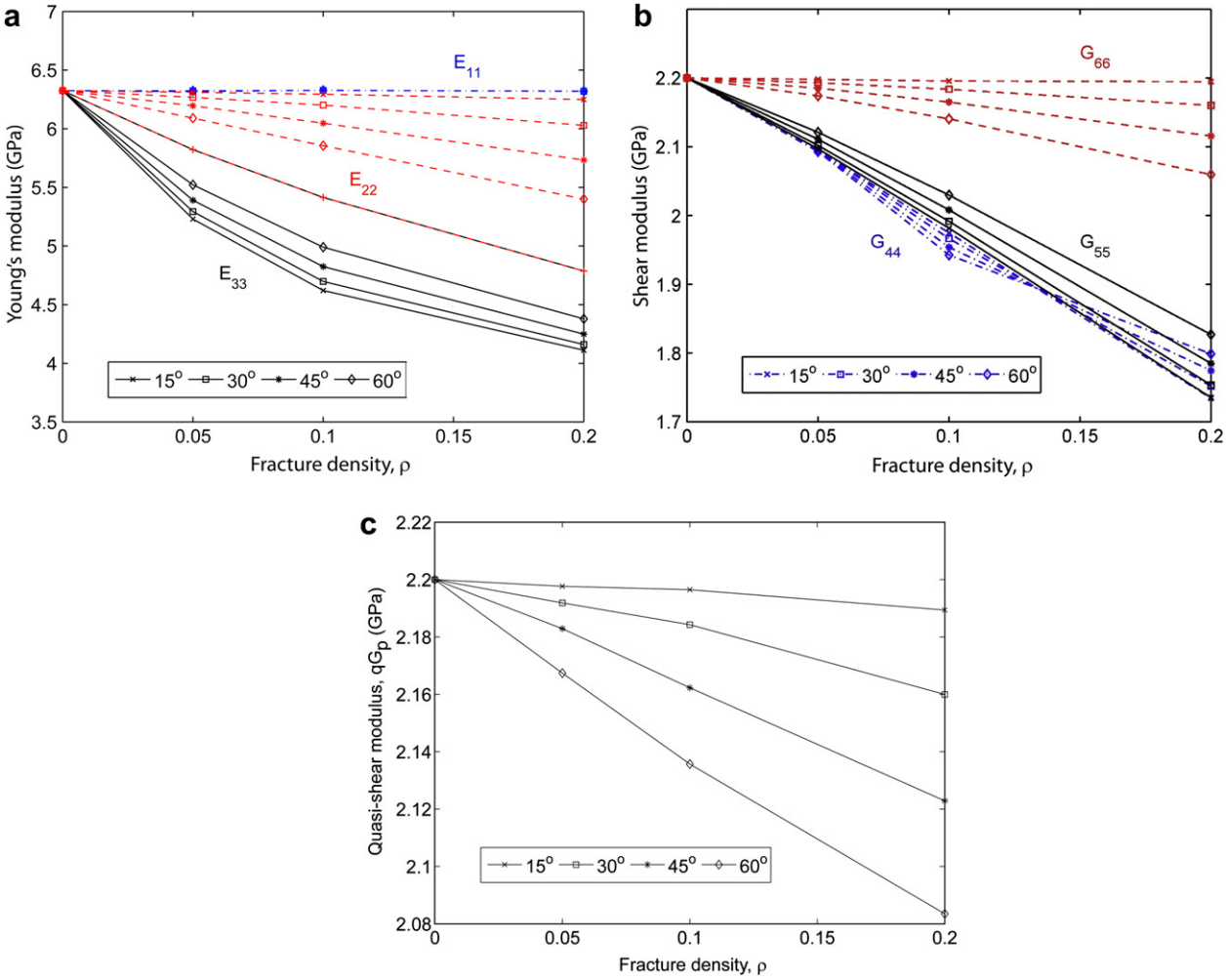

Fig. 12. Plots showing the variation in elastic moduli of rocks with prescribed fracture patterns (defined by the angle, Φ_F, between two fracture sets as 15°, 30°, 45°and 60°) and a range of fracture densities (ρ from 0.0 to 0.2). (a) The three components of the Young's moduli (E_{11}, E_{22}, and E_{33}) with increasing fracture density. The nearly horizontal solid blue line near the top represents all four E_{11} plots for the density range and for all four angles between the fracture sets (the lines just overlap). (b) The three components of the shear moduli (G_{44}, G_{55}, and G_{66}) for the four angles with increasing fracture density. (c) The quasi-shear moduli for pure shear for the same four angular configurations and density range. This moduli show the least decrease in magnitude with respect to that for no-fracture state.

modes in pristine rock within the context of the LEFM (see for example, Segall and Pollard, 1980; Du and Aydin, 1993, 1995; Crider and Pollard, 1998; De Bremaecker and Ferris, 2004). In this regard, the underlying reasoning in our approach is similar to that of the damage concept of Lyakhovsky et al. (1997); and Lyakhovsky and Ben-Zion (in review) if the fracture density is a proxy for the damage parameter in their model. On the other hand, the linkage criteria for the normal fault relays in map view investigated by Soliva and Benedicto (2004) is not quite analogous for the strike-slip fault configurations considered in our study for the simple reason that the map view of normal faults does not contain the slip vector. However, the displacement/segment separation ratio, which is a measure of the shear strain across fault steps, used by these authors to characterize various stages of fault linkage may be related to the fracture density used in our study for strike-slip fault steps. It is likely that the fracture density is related to the shear strain across the zone, however, the nature of such a possible relationship between these parameters is not yet known.

It appears that the underlying mechanical principle for fault growth processes and many of the related scaling relationships is controlled by the stress concentration at fault tips and its length dependence. First, for a simple mode II fracture, the stress components at a point in the regions away from the fracture tips decay as $(a/r)^2$ for 2D (Pollard and Segall, 1987) and $(a/r)^3$ for 3D (Ben-Zion and Sammis, 2003), where a is half fault length and r is the radial distance to the center of the fault. Second, fault interaction is an important factor in the final fault geometry of discontinuous strike-slip faults (Aydin and Schultz, 1990). It turns out that the relative locations of the neighboring fracture tips do have a strong impact on echelon mode II fracture geometry but this influence is more or less independent of the sense of echelon steps. The data on the step size and distribution are also consistent with the earlier results in that larger steps are associated with longer fault segments and, presumably, higher slip magnitudes.

Steps or relay ramps between echelon strike-slip faults include various structures (joints, pressure solutions, other faults, and folds) and eventually are cut by a through-going fault connecting the echelon fault segments. In our study area, the failure structures at steps and around the fault core are generally mode I fractures formed either under tensile local stresses (Segall and Pollard, 1980) or compressive local stresses (Horii and Nemat-Nasser, 1985). However, shear bands (Aydin et al., 2006; Shipton and Cowie, 2003) are occasionally observed at narrow contractional steps (Davatzes et al., 2003), which are neglected in this study.

Earlier experimental and theoretical studies have proposed buckling (Peng and Johnson, 1972) and bending (Renshaw and

Schulson, 2001) of thin and slender rock slabs between a set of fractures as a mechanism for through-going shear fracture formation. It is difficult to identify these mechanisms in the field. As the field data show, most fracture-bounded blocks have diamond shapes due to dihedral intersection angle between the fracture sets and may not be favorable either for buckling or bending. Rather, the triangular areas at the intersection of the fractures appear to be most prone to further fracturing and fragmentation. The rotation and translation of some fracture-bounded rock blocks with respect to the neighboring blocks can be identified in advanced stages of deformation, particularly within slivers preserved within fault cores. However, the relative timing of these rotations and relative motions with respect to the shear zone evolution cannot be determined.

The presence of multiple sets of fractures formed by splaying within fault steps and inner damage zones with intersection angles different than 90°, requires that all but the youngest set of fractures are sheared. However, it is reasonable to assume that even a sheared joint would be associated with a series of narrow pull-aparts due to common joint surface roughness introduced by hackle and rib marks. Thus, these slightly sheared joints would have collinear open fractures along their lengths and, therefore, they can be represented as a series of rectangular flat fractures for the purpose of the effective properties calculations.

The fracture intersection angles in the study area are controlled by the splay angles (Fig. 5) which show a broad range of variation (de Joussineau et al., 2007). This variation is in part due to potential interaction between closely spaced subparallel faults. For example, the average value of the splay angles is 19° for isolated single faults whereas the average splay angle reaches 50° for closely spaced interacting subparallel faults (Table 1a). It suffices to say that these average values are well within the range (15–60°) used in the effective medium models in our study. However, the effective properties based on the high end of the intersection angles (45–60°) are more appropriate for fractured slabs between closely spaced subparallel faults.

The critical fracture density of about 1.0 corresponds to the lowest vanishing values of shear moduli components (G_{55} and G_{44}) for the smallest intersection angle (15°) and one of the Young's moduli components, E_{33}, for all four intersection angles used in the modeling study. Thus, for this density, the average spacing value for one set of fractures is 5 cm for a 5 cm thick bed (see Eq. (3)) and 2.5 cm for two overlapping sets as deduced earlier. However, the problem with the critical density or spacing values is that they can never be captured in the field because once the instability is reached, the fracture systems are obliterated. We just defined an envelope by tabulating the lowest fracture spacing without disturbance or obliteration around a series of individual faults. Comparing the theoretical results with the minimum spacing range (~1–5 cm) defined by the first linear segment of the spacing distribution data from the study area (Table 1b), indicates that the calculated and measured spacing values match quite well. However, the way that fracture spacing was measured in the field is sensitive to the direction of scanline with respect to the fracture orientation. Because the scanlines are approximately perpendicular to the individual faults for single faults, and to the dominant faults for a system of faults, one set of fractures is perpendicular to this orientation and they would provide true spacing. Whereas, the other fracture set would differ from the right angle orientation to the scanline as much as the range of splay angles given in Table 1a. Considering the average values for the most common splay angles of 19–50°, the true spacing values would defer from the measured values by a factor of 0.95 and 0.64, respectively. However, the actual difference between the calculated and measured fracture spacing depends on the fracture angles from the scanline as well as their frequency as illustrated for one of the well-studied faults, the 14 m fault (Table 1, inset 2). Here more than 75% of the measured fracture angles are at high-angle (50–90°) to the scanline orientation requiring a maximum correction factor of about 0.77. Even with this correction, the theoretical and field values for the critical fracture spacing are in the same order of magnitude. These results may also imply that the lack of a large number of fracture spacing under a critical value of 1–2 cm in fault-related fracture spacing distribution plots may be due to the destruction of those fractures with spacing value equal to or smaller than that of the critical value. This type of tapering in frequency plots is commonly interpreted in terms of the minimum resolution and its impact on sampling error. Albeit, considering the minimum resolvable spacing measurement of 0.5 cm in our survey, it is likely that the initial tapering is not because of limited sampling of this range of spacing but the destruction of those fractures with spacing under a critical value.

We should also point out that cataclastic failure may occur at fracture densities corresponding to nonzero values of the moduli and having bedding interfaces fail as part of the fragmentation process which has not been considered here. The quasi-shear modulus for pure shear gives the highest critical fracture density of slightly larger than 4 for one fracture set. In light of other results, this implies that the failure will occur earlier due to weakening of the other elastic parameters for a given fracture density.

7. Conclusions

In this paper, we conceptualized fault growth in terms of increasing dimensions of fault zones with fault slip and provided examples from the same structural and lithological setting. We idealized complex fracture geometries at strike-slip fault steps and inner damage zones in order to use the effective medium models for gaining an insight in the influence of the faulting-related fractures on the mechanical properties of rocks along and around the faults. Our results indicate that a significant reduction (~20–34%) in most components of the Young's, shear, and quasi-shear (for pure shear) moduli of the fractured rock masses should occur as the fracture density increases modestly. The extrapolated values of the Young's and shear moduli for the fracture configuration which resulted in the greatest moduli reduction would suggest an upper bound value for a critical density of about 1. This corresponds to a critical fracture spacing value on the order of 5 cm for a bed thickness of 5 cm for one set, and 2.5 cm for two overlapping sets. The spacing values defined by the minimum values associated with the line fit to the lower ends of the measured spacing distributions from the study area suggest that the undisturbed smallest fracture spacing is about 1–2 cm with a possible correction factor of 0.77, which still amounts to the same order of magnitude as the modeling results. This also implies that the lack of a large number of fracture spacing below 1–2 cm in fault-related fracture spacing distribution plots may be due to the destruction of most fractures with spacing under a critical fracture spacing value.

Acknowledgements

The works at the Valley of Fire State Park by many former graduate students and postdocs who studied with A. Aydin at Stanford University formed the foundation for establishing the conceptual models in this paper. Among these, Ghislain de Joussineau's work has been heavily relied upon. A partial list of other students and postdocs includes R. Myers, E. Flodin, N. Davatzes, and P. Eichhubl. A. Aydin is supported by the US DOE Basic Energy Science, Division of Chemical Sciences, Geosciences and Bio-Sciences, Grant no. DE-FG03-94ER14462. Work of J.G. Berryman performed under auspices of the US DOE by the University of

California Lawrence Berkeley National Laboratory under contract no. DE-ACO2-05CH11231. A. Aydin is grateful to the Valley of Fire State Park personnel for their support of the field campaigns through many years. Comments by Christopher Wibberley, Roy Schliche, Zoe Shipton, and Roger Soliva improved the manuscript.

References

Agosta, F., Aydin, A., 2006. Architecture and deformation mechanism of a basin bounding normal fault in Mesozoic platform carbonates, central Italy. Journal of Structural Geology 28, 2445–2467.

Aki, K., 1989. Geometric features of a fault zone related to the nucleation and termination of an earthquake rupture, in: Proceedings of Conference XLV Fault Segmentation and Controls of Rupture Initiation and Termination. US Geological Survey Open File Report 89-315, pp. 1–9.

Aydin, A., 2000. Fractures, faults, and hydrocarbon entrapment, migration and flow. Marine and Petroleum Geology 17, 797–814.

Aydin, A., Nur, A., 1982. Evolution of pull-apart basins and their scale independence. Tectonics 1, 91–105.

Aydin, A., Schultz, R.A., 1990. Effect of mechanical interaction on the development of strike-slip faults with echelon patterns. Journal of Structural Geology 12, 123–129.

Aydin, A., Borja, R.I., Eichhubl, P., 2006. Geological and Mathematical Framework for failure modes in granular rock. Journal of Structural Geology 28, 83–98.

Backus, G.E., 1962. Long-wave elastic anisotropy produced by horizontal layering. Journal of Geophysical Research 67, 4427–4440.

Bai, T., Pollard, D.D., 2000. Fracture spacing in layered rocks: a new explanation based on the stress transition. Journal of Structural Geology 22, 43–57.

Barka, A., Kadinsky-Cade, K., 1988. Strike-slip fault geometry in Turkey and its influence on earthquake activity. Tectonics 7, 663–684.

Ben-Zion, Y., Sammis, C.G., 2003. Characterization of fault zones. Pure and Applied Geophysics 160, 677–715. 0033–4553/03/040677-39.

Berryman, J.G., 2008. Elastic and transport properties in polycrystals of cracked grains: cross-property relations and microstructure. International Journal of Engineering Science 46, 500–512.

Berryman, J.G., Aydin, A., Quasi-static analysis of elastic behaviour for some higher density crack systems. International Journal of Numerical and Analytical Methods in Geomechanics, in press, doi:10.1002/nag.874.

Berryman, J.G., Grechka, V., 2006. Random polycrystals of grains containing cracks: Model of quasistatic elastic behavior for fractured systems. Journal of Applied Physics 100, 113527.

Bohannon, R.G., 1983. Mesozoic and Cenozoic tectonic development of the Muddy, North Muddy, and northern Black Mountains, Clark County, Nevada. In: Miller, D.M., Todd, V.R., Howard, K.A. (Eds.), Tectonic and Stratigraphic Studies in the Eastern Great Basin. Geological Society of America Memoir, 157, pp. 125–148.

Bristow, J., 1960. Microcracks and the static and dynamic elastic constants of annealed and heavily cold-worked metals. British Journal of Applied Physics 11, 81–85.

Budiansky, B., O'Connell, R.J., 1976. Elastic moduli of a cracked solid. International Journal of Solids and Structures 12, 81–97.

Burgmann, R., Pollard, D.D., 1994. Strain accommodation about strike-slip fault discontinuities in granitic rock under brittle-to-ductile conditions. Journal of Structural Geology 16, 1655–1674.

Çakir, M., Aydin, A., 1994. Tectonics and Fracture Characteristics of the Northern Lake Mead, SE Nevada, Field Guide Book. Proceedings of the Stanford Rock Fracture Project Workshop.

Çakir, M., Aydin, A., Campagna, D.J., 1998. Deformation pattern around conjoining strike-slip faults systems in the Basin and Range, southeast Nevada: the role of strike-slip faulting in basin formation and inversion. Tectonics 17, 344–359.

Cartwright, J.A., Trudgill, B.D., Mansfield, C.S., 1995. Fault growth by segment linkage: an explanation for scatter in maximum displacement and trace length data from the Canyonlands Grabens of SE Utah. Journal of Structural Geology 17, 1319–1326.

Childs, C., Manzocchi, T., Walsh, J.J., Bonson, C.G., Nicol, A., Schopfer, M.P.J., 2009. A geometric model of fault zone and fault rock thickness variations. Journal of Structural Geology 31 (2), 117–127.

Cowie, P.A., Scholz, C.H., 1992. Displacement-length scaling relationship for faults: data synthesis and discussion. Journal of Structural Geology 14, 1149–1156.

Cox, S.J.D., Scholz, C.H., 1988. Rupture initiation in shear fracture of rocks: an experimental study. Journal of Geophysical Research 93, 3307–3320.

Crider, J.G., Pollard, D.D., 1998. Fault linkage: three-dimensional mechanical interaction between echelon normal faults. Journal of Geophysical Research 103, 24373–24391.

Davatzes, N.C., Aydin, A., 2004. Fault linkage and evolution of the fault core in sandstone, Valley of Fire State Park, Nevada: a preliminary report. Rock Fracture Project Workshop Vol. 15, E1–E10.

Davatzes, N.C., Aydin, A., Eichhubl, P., 2003. Overprinting faulting mechanisms during the development of multiple fault sets in sandstone, Chimney Rock, Utah. Tectonophysics 363, 1–18.

Dawers, N.H., Anders, M.H., 1995. Displacement-length scaling and fault linkage. Journal of Structural Geology 17, 607–614.

De Bremaecker, J.-C., Ferris, M.C., 2004. Numerical models of shear fracture propagation. Engineering Fracture Mechanics 71, 2161–2178.

de Joussineau, G., Aydin, A., 2007. The evolution of the damage zone with fault growth and its multiscale characterization. Journal of Geophysical Research 112, B12401,. doi:10.1029/2006JB004711.

de Joussineau, G., Aydin, A., 2009. Segmentation along strike-slip faults and their self-similar architecture. Pure and Applied Geophysics 166, 1575–1594. doi:10.1007/s00024-009-0511-4.

de Joussineau, G., Mutlu, O., Aydin, A., Pollard, D.D., 2007. Characterization of strike-slip fault-splay relationships in sandstone. Journal of Structural Geology 29, 1831–1842.

Dewey, J.W., 1976. Seismicity of Northern Anatolia. Bulletin Seismological Society of America 66, 843–868.

Du, Y., Aydin, A., 1993. The maximum distortional strain energy density criterion for shear fracture propagation with applications to the growth paths of *en echelon* faults. Geophysical Research Letters 20, 1091–1094.

Flodin, E.A., Aydin, A., 2004. Evolution of a strike-slip fault network, Valley of Fire, southern Nevada. Geological Society of America Bulletin 116, 42–59. doi:10.1130/B25282.1.

Flodin, E.A., Gerdes, M., Aydin, A., Wiggins, W.D., 2005. Petrophysical properties of cataclastic fault rock in sandstone. In: Sorkhabi, R., Tsuji, Y. (Eds.), Faults, Fluid Flow, and Petroleum Traps. American Association of Petroleum Geologists Memoir, 85, pp. 197–227.

Gamond, J.F., 1983. Displacement features associated with fault zones: a comparison between observed examples and experimental models. Journal of Structural Geology 5, 33–45.

Grechka, V., Kachanov, M., 2006. Seismic characterization of multiple fracture sets: Does orthotropy suffice? Geophysics 71, D93–D105.

Griffith, W.A., Sanz, P.F., Pollard, D.D., 2009. Influence of fault damage zone fractures on the effective stiffness of fault damage zone rocks. Pure and Applied Geophysics 166, 1595–1627, doi:10.1007/s00024-009-0519-9.

Harris, R.A., Day, S.M., 1999. Dynamic 3D simulation of earthquakes on en echelon faults. Geophysical Research Letters 26, 2089–2092.

Harris, R.A., Archuleta, R.J., Day, S.M., 1999. Fault steps and the dynamic rupture process: 2-d simulation of a spontaneously propagating shear fractures. Geophysical Research Letters 18, 893–896.

Holt, R.M., Ingsøy, P., Mikkelsen, M., 1987. Rock mechanical analysis of North Sea reservoir formations. SPE #16796. 62nd Annual Technical Conference, Dallas, TX.

Horii, H., Nemat-Nasser, S., 1985. Compression-induced microcrack growth in brittle solids: axial splitting and shear fracture. Journal of Geophysical Research 90, 3105–3125.

Hull, J., 1988. Thickness-displacement relationships for deformation zones. Journal of Structural Geology 10, 431–435.

Kim, Y., Peacock, D.C.P., Sanderson, D.J., 2004. Fault damage zones. Journal of Structural Geology 26, 503–517.

Knott, S.D., Beach, A., Brockbank, P.J., McCallum, J.E., Welbon, A.I., 1996. Spatial and mechanical controls on normal fault population. Journal of Structural Geology 18, 359–372.

Lawn, B.R., Wilshaw, T.R., 1975. Fracture of Brittle Solids. Cambridge University Press, 204 pp.

Le Pichon, X., Şengör, A.M.C., Demirbağ, E., Rangin, C., İmren, C., Armijo, R., Görür, N., Çağatay, N., Mercier de Lepinay, B., Meyer, B., Saatçilar, R., Tok, B., 2001. The active Main Marmara Fault. Earth and Planetary Sciences Letters 192, 595–616.

Lockner, D.A., Madden, T.R., 1991. A multiple-crack model of brittle fracture 1. Non-time-dependent simulations. Journal of Geophysical Research 96, 19623–19642.

Lyakhovsky, V., Ben-Zion, Y., in review. Evolving fault zone structures in a damage rheology model. *Geochemistry, Geophysics, Geosystems*, in review.

Lyakhovsky, V., Ben-Zion, Y., Agnon, A., 1997. Distributed damage, faulting, and friction. Journal of Geophysical Research 102, 27635–27649.

Martel, S.J., 1990. Formation of compound strike-slip fault zones, Mount Abbot quadrangle, California. Journal of Structural Geology 12, 869–882.

Martel, S.J., Peterson Jr., J.E., 1991. Interdisciplinary characterization of fracture systems at the US/BK site, Grimsel Laboratory, Switzerland. International Journal of Rock Mechanics and Mining Science and Geomechanical Abstracts 28, 259–323.

Martel, S.J., Pollard, D.D., Segall, P., 1988. Development of simple strike-slip fault zones in granitic rock, Mount Abbot quadrangle, Sierra Nevada, California. Geological Society of America Bulletin 99, 1451–1465.

Myers, R., 1999. Structure and hydraulics of brittle faults in sandstone, PhD thesis, Stanford University.

Myers, R., Aydin, A., 2004. The evolution of faults formed by shearing across joint zones in sandstone. Journal of Structural Geology 26, 947–966.

Nye, J.F., 1985. Physical Properties of Crystals: Their Representation by Tensors and Matrices. Oxford Science Publications.

Odling, N.E., Harris, S.D., Knipe, R.J., 2004. Permeability scaling properties of fault damage zones in siliclastic rocks. Journal of Structural Geology 26, 1727–1747.

Otsuki, K., Dilov, T., 2005. Evolution of self-similar geometry of experimental fault zones; implications for seismic nucleation and earthquake size. Journal of Geophysical Research 110, B03303. doi:10.1029/2004JB003359.

Pachell, M.A., Evans, J.P., 2002. Growth, linkage, and termination processes of a 10-km-long strike-slip fault in jointed granite: the Gemini fault zone, Sierra Nevada, California. Journal of Structural Geology 24, 1903–1924.

Palchik, V., 1999. Influence of porosity and elastic modulus on uniaxial strength in soft brittle porous sandstone. Rock Mechanics and Rock Engineering 32, 303–309.
Peacock, D.C.P., Sanderson, D.J., 1991. Displacement, segment linkage and relay ramps in normal fault zones. Journal of Structural Geology 13, 721–733.
Peacock, D.C.P., Sanderson, D.J., 1995. Strike-slip relay ramps. Journal of Structural Geology 17, 1351–1360.
Peng, S., Johnson, A.M., 1972. Crack growth and faulting in cylindrical specimens of Chelmsford Granite. International Journal of Rock Mechanics. Mineral Sciences and Geomechanics Abstracts 9, 37–86.
Pollard, D.D., Fletcher, R.C., 2005. Fundamentals of Structural Geology. Cambridge University Press, Cambridge, UK, 500 pp.
Pollard, D.D., Segall, P., 1987. Theoretical displacements and stresses near fractures in rock: with applications to faults, joints, veins, dikes, and solution surfaces. In: Atkinson, B.K. (Ed.), Fracture Mechanics of Rock. Academic Press, London, pp. 277–349.
Reches, Z., Lockner, D.A., 1994. Nucleation and growth of faults in brittle rocks. Journal of Geophysical Research 99, 18159–18173.
Renshaw, C.E., Schulson, E.M., 2001. Universal behaviour in compressive failure of brittle materials. Nature 412, 897–899.
Rispoli, R., 1981. Stress fields about strike-slip faults inferred from stylolites and tension gashes. Tectonophysics 75, 729–736.
Robertson, E.C., 1983. Relationship of fault displacement to gouge and breccia thickness. Mineral Engineering Transactions. American Institute of Mining Engineering 35, 1426–1432.
Sayers, C.M., Kachanov, M., 1991. A simple technique for finding effective elastic constants of cracked solids for arbitrary crack orientation statistics. International Journal of Solids and Structures 27, 671–680.
Schlische, R.W., Young, S.S., Ackermann, R.V., Gupta, A., 1996. Geometry and scaling relations of a population of very small rift-related normal faults. Geology 24, 683–686.
Schoenberg, M., Muir, F.A., 1989. A calculus for finely layered anisotropic media. Geophysics 54 581–489.
Scholz, C.H., 2002. The Mechanics of Earthquakes and Faulting, second ed. Cambridge University Press, Cambridge, UK, 471 pp.
Segall, P., Pollard, D.D., 1980. Mechanics of discontinuous faults. Journal of Geophysical Research 85, 4337–4350.
Segall, P., Pollard, D.D., 1983. Nucleation and growth of strike slip faults in granite. Journal of Geophysical Research 88, 555–568.
Shaw, B.E., Dieterich, J.H., 2007. Probabilities for jumping fault segment stepovers. Geophysical Research Letters 34, L01307. doi:10.1029/2006GL027980.
Shipton, Z.K., Cowie, P.A., 2003. A conceptual model for the origin of fault damage zone structures in high-porosity sandstone. Journal of Structural Geology 25, 333–344.
Sibson, R.H., 1985. Stopping of earthquake ruptures at dilational fault jogs. Nature 316, 248–251.
Sibson, R.H., 1986. Structural permeability of fluid-driven fault-fracture meshes. Journal of Structural Geology 18, 1031–1042.
Soliva, R., Benedicto, A., 2004. A linkage criterion for segmented normal faults. Journal of Structural Geology 26, 2251–2267.
Stein, R.S., Barka, A.A., Dieterich, J.H., 1997. Progressive failure on the North Anatolian fault since 1939 by earthquake stress triggering. Geophysical Journal International 128, 594–604.
Stirling, M.W., Wesnousky, S.G., Shimazaki, K., 1996. Fault trace complexity, cumulative slip, and the shape of the magnitude-frequency distribution for strike-slip faults: a global survey. Geophysical Journal International 124, 833–868.
Toksöz, N., Shakal, A.F., Michael, A.J., 1979. Space-time migration of earthquakes along the North Anatolian fault zone and seismic gap. Pure and Applied Geophysics 117, 1258–1270.
Walsh, J.J., Watterson, J., 1987. Distribution of cumulative displacement and seismic slip on a single normal fault surface. Journal of Structural Geology 9, 1039–1046.
Watterson, J., 1986. Fault dimensions, displacement and growth. Pure and Applied Geophysics 124, 365–373.
Wesnousky, S.G., 1988. Seismological and structural evolution of strike-slip faults. Nature 335, 340–342.
Wesnousky, S.G., 2006. Predicting the endpoints of earthquake ruptures. Nature 444, 358–360.
Willemse, E.J.M., Peacock, D.C.P., Aydin, A., 1997. Nucleation and growth of strike-slip faults in limestones from Somerset, U.K. Journal of Structural Geology 19, 1461–1477.
Wu, H., Pollard, D.D., 1995. An experimental study of the relationship between joint spacing and layer thickness. Journal of Structural Geology 17, 887–905.